JACS
JOURNAL OF THE AMERICAN CHEMICAL SOCIETY
Article
pubs.acs.org/JACS

Determining the Role of Polymer Molecular Weight for High-Performance All-Polymer Solar Cells: Its Effect on Polymer Aggregation and Phase Separation

Hyunbum Kang,[||,†] Mohammad Afsar Uddin,[||,‡] Changyeon Lee,[†] Ki-Hyun Kim,[†] Thanh Luan Nguyen,[‡] Wonho Lee,[†] Yuxiang Li,[‡] Cheng Wang,[§] Han Young Woo,*[,‡] and Bumjoon J. Kim*[,†]

[†]Department of Chemical and Biomolecular Engineering, Korea Advanced Institute of Science and Technology (KAIST), 335 Gwahangno, Yuseong, Daejeon 305-701, Korea

[‡]Department of Nanofusion Engineering, Department of Cogno-Mechatronics Engineering, Pusan National University, Miryang 627-706, Korea

[§]Advanced Light Source, Lawrence Berkeley National Laboratory, Berkeley, California 94720, United States

Supporting Information

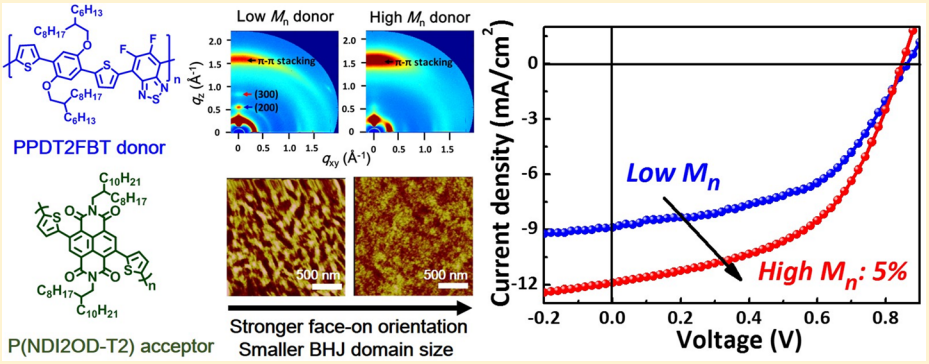

ABSTRACT: The molecular weight of a conjugated polymer is one of the key factors determining the electrical, morphological, and mechanical properties as well as its solubility in organic solvents and miscibility with other polymers. In this study, a series of semicrystalline poly[(2,5-bis(2-hexyldecyloxy)phenylene)-*alt*-(5,6-difluoro-4,7-di(thiophen-2-yl)benzo[*c*][1,2,5]thiadiazole)] (PPDT2FBT) polymers with different number-average molecular weights (M_n's) (**PPDT2FBT$_L$**, M_n = 12 kg/mol; **PPDT2FBT$_M$**, M_n= 24 kg/mol; **PPDT2FBT$_H$**, M_n= 40 kg/mol) were synthesized, and their photovoltaic properties as electron donors for all-polymer solar cells (all-PSCs) with poly[[*N*,*N*′-bis(2-octyldodecyl)-napthalene-1,4,5,8-bis(dicarboximide)-2,6-diyl]-*alt*-5,5′-(2,2′-bithiophene)] (P(NDI2OD-T2)) acceptor were studied. The M_n effect of PPDT2FBT on the structural, morphological, electrical, and photovoltaic properties was systematically investigated. In particular, tuning the M_n induced dramatic effects on the aggregation behaviors of the polymers and their bulk heterojunction morphology of all-PSCs, which was thoroughly examined by grazing incident X-ray scattering, resonant soft X-ray scattering, and other microscopy measurements. High M_n **PPDT2FBT$_H$** promoted a strong "face-on" geometry in the blend film, suppressed the formation of an excessively large crystalline domain, and facilitated molecularly intermixed phases with P(NDI2OD-T2). Therefore, the optimized all-PSCs based on **PPDT2FBT$_H$**/P(NDI2OD-T2) showed substantially higher hole and electron mobilities than those of **PPDT2FBT$_L$**/P(NDI2OD-T2), leading to a power conversion efficiency exceeding 5%, which is one of the highest values for all-PSCs reported thus far.

INTRODUCTION

All-polymer solar cells (all-PSCs), which are composed of binary blends of conjugated polymer donor and acceptor, offer several advantages over conventional polymer donor/fullerene-based PSCs. These advantages include enhanced light absorption, extensive tunability of their energetic and chemical properties, and superior chemical and mechanical stability.[1−13] Significant efforts have been devoted to the development of new polymer acceptors with high electron mobility, such as perylene diimide (PDI)[7,14] and naphthalene diimide (NDI)[6,9]-based copolymers to enhance the device performance of all-PSCs. In addition, the choice of processing solvents and solvent additives can control the bulk heterojunction (BHJ) morphology of all-PSCs, and the crystalline behavior of the polymer chains.[4,6,9,11,15] Despite these efforts to optimize all-PSCs, less success has been achieved for all-PSCs than for polymer/fullerene PSC systems. Indeed, few papers have reported all-

Received: December 3, 2014
Published: January 21, 2015

DOI: 10.1021/ja5123182
J. Am. Chem. Soc. 2015, 137, 2359−2365

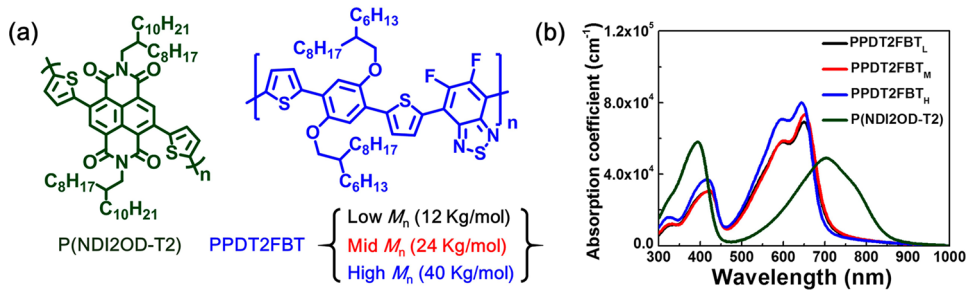

Figure 1. (a) Molecular structure of P(NDI2OD-T2) and PPDT2FBT. (b) UV−vis spectra of PPDT2FBT and P(NDI2OD-T2) polymers.

PSCs with power conversion efficiencies (PCEs) of more than 4%.[3,7,9−11] Their relatively low PCEs are due mainly to the undesirable features of the BHJ blend morphology, including large-scale phase-separated domain, reduced ordering of polymer chains, and inhomogeneous internal phase composition.[15−17] In particular, optimizing the BHJ morphology of all-PSCs is a great challenge because of the significantly reduced entropic contribution to the Gibbs free energy, which favors the demixing of the two different polymers.[18] In addition, the importance of the desired blend morphology for efficient exciton dissociation and charge transport would be amplified greatly because the electron mobility of the polymer acceptors is typically much lower than that of fullerene derivatives.[9,19]

The molecular weight of conjugated polymers is a key factor in determining their electrical, structural, and mechanical properties. In addition, their solubility in processing solvents and polymer blend phase behavior are strongly affected by molecular weight. Considerable efforts have been made to determine the relationship between the molecular weight of the conjugated polymers and the performance of organic field effect transistors and polymer/fullerene-based PSCs.[20−26] For example, the regioregular poly(3-hexylthiophene) with a high molecular weight was beneficial in promoting their intermolecular charge transport and enhancing the hole mobility due to the high interconnectivity between the crystalline grains of the polymers.[21] In addition, for low bandgap polymer/fullerene-based PSC systems,[26−28] the use of higher molecular weight polymers often induced better charge transport and device performance. However, very limited studies have been reported related to the molecular weight effect of the photovoltaic polymers in all-PSCs.[29] In addition, the influence of the molecular weight on the microstructure of the polymers and the BHJ morphology in the all-PSCs is poorly understood.

Herein, we report highly efficient all-PSCs showing greater than 5% PCE by utilizing poly[(2,5-bis(2-hexyldecyloxy)-phenylene)-*alt*-(5,6-difluoro-4,7-di(thiophen-2-yl)benzo[*c*]-[1,2,5]thiadiazole)] (PPDT2FBT) as the electron donor and poly[[*N*,*N*′-bis(2-octyldodecyl)-napthalene-1,4,5,8-bis-(dicarboximide)-2,6-diyl]-*alt*-5,5′-(2,2′-bithiophene)] (P(NDI2OD-T2)) as an electron acceptor (Figure 1a). To establish clear structure−property−performance correlations in terms of the molecular weight of the conjugated polymer in all-PSCs, we developed a series of PPDT2FBT polymers with different number-average molecular weights (M_n's) of 12, 24, and 40 kg/mol and investigated their photovoltaic performances. In particular, tuning the M_n value induced dramatic effects on the crystalline behaviors of the polymers and their BHJ morphology blended with the semicrystalline polymer acceptor, P(NDI2OD-T2). The use of the high M_n PPDT2FBT polymers induced a strong "face-on" geometry in the active layer, suppressed the formation of overly large crystalline domains, and produced molecularly intermixed phases with P(NDI2OD-T2) for efficient exciton dissociation and charge generation.

RESULTS AND DISCUSSION

A series of PPDT2FBT polymers with different M_n values of 12, 24, and 40 kg/mol were synthesized by the Stille coupling of 4,7-bis(5-trimethylstannylthiophen-2-yl)-5,6-difluoro-2,1,3−benzothiadiazole and 1,4-dibromo-2,5-bis(2-hexyldecyloxy)-benzene with $Pd_2(dba)_3$ as a catalyst in chlorobenzene using a microwave reactor (Figure 1a and Supporting Information (SI) Table S1).[30] The terms were defined according to M_n: **PPDT2FBT$_L$**, M_n = 12 kg/mol; **PPDT2FBT$_M$**, M_n = 24 kg/mol; **PPDT2FBT$_H$**, M_n = 40 kg/mol. A photovoltaic polymer, PPDT2FBT, was reported as an efficient polymer donor in polymer/fullerene based PSC, showing prominent crystalline organization via noncovalent intra- and interchain hydrogen bonds and dipole−dipole interactions.[30] Semicrystalline P-(NDI2OD-T2) was synthesized using the method reported in the literature and used as an n-type polymer because of its high electron mobility and electron affinity.[31,32] The PPDT2FBT and P(NDI2OD-T2) polymers have the lowest unoccupied molecular orbital/highest occupied molecular orbital (LUMO/HOMO) levels of −3.7 eV/−5.5 eV[30] and −4.3 eV/−5.9 eV,[33] respectively, which produce well-matched energy level alignment with the energy offsets of LUMO−LUMO (0.6 eV for electron transfer) and HOMO−HOMO (0.4 eV for hole transfer). The optical properties of the PPDT2FBT polymers with different M_n were characterized by thin-film UV−vis spectroscopy, as shown in SI Table S1 and Figure 1b. Increasing the M_n resulted in small enhancement of the absorption coefficients in the film (from ∼7 × 10^4 /cm for **PPDT2FBT$_L$** to ∼8 × 10^4 /cm for **PPDT2FBT$_H$**), but the difference was not significant.[27,28]

Conventional-type all-PSCs with a device configuration of ITO/PEDOT:PSS/PPDT2FBT:P(NDI2OD-T2)/LiF:Al were fabricated to examine the M_n effects of PPDT2FBT on the photovoltaic characteristics in all-PSCs. (Detailed procedures for device fabrication are described in the SI.) Initially, to elucidate the M_n effects on the device performance, the devices were prepared under identical conditions without thermal- or solvent-additive treatments. The optimized PPDT2FBT:P-(NDI2OD-T2) blend ratio was 1.0:0.7 (w/w), and the optimized film thickness of the active layer spun-cast from a chloroform (CF) solution was approximately 90−100 nm, irrespective of the M_n of the PPDT2FBT polymers. Figure 2 shows the *J*−*V* curves and the external quantum efficiency (EQE) of the PPDT2FBT:P(NDI2OD-T2)-based all-PSCs. Table 1 summarizes the photovoltaic parameters of all-PSC

DOI: 10.1021/ja5123182
J. Am. Chem. Soc. 2015, 137, 2359−2365

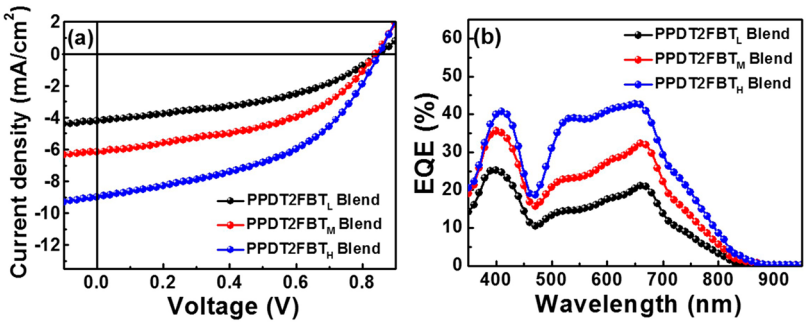

Figure 2. (a) $J-V$ characteristics and (b) EQE spectra of PPDT2FBT:P(NDI2OD-T2)-based all-PSCs.

Table 1. Photovoltaic Parameters of PPDT2FBT:P(NDI2OD-T2)-Based All-PSCs

polymer	V_{oc} (V)	J_{sc} (mA cm^{-2})	FF	PCE$_{max}$ (%)	EQE$_{max}$ (%)	calcd J_{sc} (mA cm^{-2})
PPDT2FBT$_L$	0.85	4.22	0.43	1.54 (1.42)[a]	25.3	4.06
PPDT2FBT$_M$	0.84	6.16	0.46	2.39 (2.28)[a]	35.6	6.23
PPDT2FBT$_H$	0.85	8.98	0.47	3.59 (3.48)[a]	42.8	8.74

[a]The average PCE values were obtained from more than 10 separate devices.

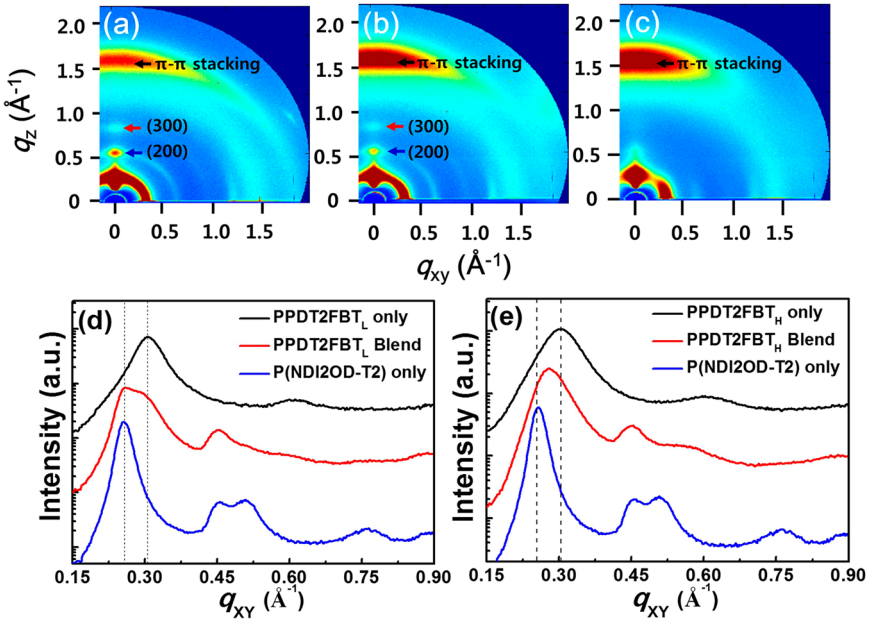

Figure 3. 2D GIXS patterns of PPDT2FBT pristine films with different M_n: (a) PPDT2FBT$_L$, (b) PPDT2FBT$_M$, and (c) PPDT2FBT$_H$. Linecuts of GIXS patterns for (d) PPDT2FBT$_L$:P(NDI2OD-T2) and (e) PPDT2FBT$_H$:P(NDI2OD-T2) blend films.

devices. The **PPDT2FBT$_L$**- and **PPDT2FBT$_M$**-based devices yielded PCEs of 1.54% and 2.39% with open-circuit voltage (V_{OC}) of 0.85 and 0.84 V, short-circuit current density (J_{SC}) of 4.22 and 6.16 mA cm^{-2}, and fill factor (FF) of 0.43 and 0.46, respectively. Interestingly, among the three PPDT2FBT-based all-PSCs, the **PPDT2FBT$_H$**:P(NDI2OD-T2)-based all-PSC showed the best PCE value of 3.59% (V_{OC}, 0.85 V; J_{SC}, 8.98 mA cm^{-2}; and FF, 0.47). This dramatic enhancement in the PCE values in the **PPDT2FBT$_H$**-based device was due mainly to the substantial increase in the J_{SC} value. In addition, the changes in the J_{SC} values for the PPDT2FBT-devices with different M_n values were well-reflected in the changes of their spectral responses shown in the EQE curves. For example, as the M_n of PPDT2FBT increased, the maximum EQE (EQE$_{max}$) of the PPDT2FBT:P(NDI2OD-T2)-based all-PSCs increased remarkably from 25.3% for **PPDT2FBT$_L$** to 42.8% for **PPDT2FBT$_H$**.

Grazing incidence X-ray scattering (GIXS) and resonant soft X-ray scattering (R-SoXS) measurements were performed to examine the crystalline ordering and the blend morphology of the PPDT2FBT:P(NDI2OD-T2) polymers as a function of M_n. First, the GIXS results of the pristine **PPDT2FBT$_L$**, **PPDT2FBT$_M$**, and **PPDT2FBT$_H$** polymer films were compared. The three polymers showed a similar (100) peak position in the in-plane direction with a lamellar spacing of 2.1 nm (q = 0.30 Å^{-1}), and the (010) peak was also measured using a $\pi-\pi$ stacking distance of 0.37 nm (q = 1.69 Å^{-1}), as shown in Figure 3 and SI Figure S1. However, the distinct differences in the detailed microstructure and crystalline orientation of the PPDT2FBT polymer films were observed depending on their M_n values. First, **PPDT2FBT$_L$** had the strongest (100), (200), and (300) peaks with significantly more pronounced reflections in both the in-plane and out-of-plane directions compared to **PPDT2FBT$_L$** and **PPDT2FBT$_H$**. Indeed, the peak intensity

DOI: 10.1021/ja5123182
J. Am. Chem. Soc. 2015, 137, 2359−2365

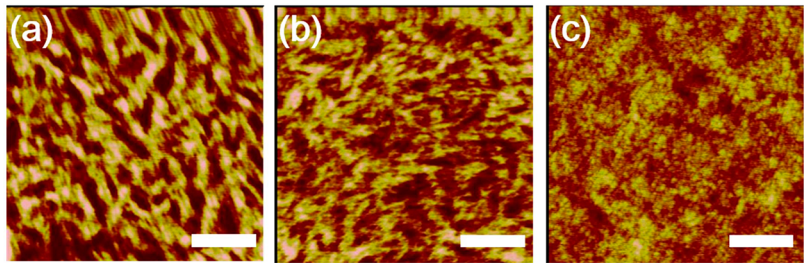

Figure 4. AFM height images of (a) **PPDT2FBT$_M$**:P(NDI2OD-T2) (rms roughness = 1.9 nm), (b) **PPDT2FBT$_M$**:P(NDI2OD-T2) (rms roughness = 1.2 nm), and (c) **PPDT2FBT$_H$**:P(NDI2OD-T2) (rms roughness = 0.8 nm). Scale bars are 500 nm.

was gradually decreased with increasing M_n value, suggesting that **PPDT2FBT$_L$** had the strongest crystalline order. This was also supported by calculations of the crystalline correlation length (D_{100}) of the polymers using the Scherrer equation (SI Table S1).[34−36] The D_{100} values provide a measurement of the distance over which the crystalline order was preserved. As the M_n decreased, the D_{100} value significantly increased from 7.66 (**PPDT2FBT$_H$**), to 10.47 nm (**PPDT2FBT$_M$**), to 11.02 nm (**PPDT2FBT$_L$**). On the other hand, **PPDT2FBT$_L$** had more randomly oriented crystallites compared to **PPDT2FBT$_M$** and **PPDT2FBT$_H$**, showing that both the (100) and (010) peaks of **PPDT2FBT$_L$** were smeared into strong arc shapes with wide angular distributions. In contrast, the trend to form an angular distribution was reduced substantially for higher M_n **PPDT2FBT$_H$**. The relative peak intensities of in-plane and out-of-plane (100) scattering ($(100)_{in}/(100)_{out}$) for the **PPDT2FBT$_L$**, **PPDT2FBT$_M$** and **PPDT2FBT$_H$** polymer films were also compared,[37] and **PPDT2FBT$_H$** showed a significantly higher value than **PPDT2FBT$_M$** and **PPDT2FBT$_L$**. Therefore, the degree of crystalline ordering of PPDT2FBT was reduced significantly with increasing M_n, but **PPDT2FBT$_H$** had a greater preference for the "face-on" molecular orientation. Figure 3d,e and SI Figures S2 and S3 compare the GIXS patterns of the PPDT2FBT:P(NDI2OD-T2) blends with different M_n of PPDT2FBT under the optimized device conditions. Interestingly, similar trends in crystalline ordering as a function of M_n were measured for the pristine PPDT2FBT polymers and the PPDT2FBT:P(NDI2OD-T2) blend films. As shown in SI Figure S2a−c, although all the blends had a preferential face-on orientation, the **PPDT2FBT$_L$**:P(NDI2OD-T2) blend film had more randomly oriented crystallites relative to **PPDT2FBT$_H$**:P(NDI2OD-T2).

The **PPDT2FBT$_L$**:P(NDI2OD-T2) blend film showed two distinct peaks of q = 0.25 Å^{-1} and q = 0.31 Å^{-1} for $(100)_{in}$ scattering in the in-plane direction (Figure 3d). The first diffraction peak at q = 0.25 Å^{-1} is characteristic of P(NDI2OD-T2), whereas the second diffraction peak at q = 0.31 Å^{-1} originates from **PPDT2FBT$_L$**. In contrast, the **PPDT2FBT$_H$**:P(NDI2OD-T2) blend showed a single $(100)_{in}$ diffraction peak at q = 0.28 Å^{-1}, which resulted from the overlap of two different $(100)_{in}$ peaks of pristine P(NDI2OD-T2) (at q = 0.25 Å^{-1}) and **PPDT2FBT$_H$** (at q = 0.31 Å^{-1}). The peak intensity of low M_n **PPDT2FBT$_L$** was much stronger than that of **PPDT2FBT$_H$** while its peak width was significantly narrower than that of **PPDT2FBT$_H$**. Therefore, the scattering peak of **PPDT2FBT$_L$** may become clearly distinguishable from the P(NDI2OD-T2) peak in the **PPDT2FBT$_L$**:P(NDI2OD-T2) blend film. This phenomenon was also observed in the highly crystalline P3HT:P(NDI2OD-T2) blends.[15,38,39] This difference in the tendency for the formation of pure **PPDT2FBT** crystalline phase in PPDT2FBT:P(NDI2OD-T2) blend with changing M_n was visualized by comparing the atomic force microscopy (AFM) images (Figure 4). The formation of distinct PPDT2FBT domains in the PPDT2FBT:P(NDI2OD-T2) blends was observed when the M_n of PPDT2FBT was decreased. Figure 4a shows large aggregates of **PPDT2FBT$_L$** with much reduced interfacial area, which is in stark contrast to the significantly finer domains of **PPDT2FBT$_H$**:P(NDI2OD-T2) (Figure 4c). In addition, both the mean domain size and the surface roughness of the PPDT2FBT:P(NDI2OD-T2) blends decreased progressively as the M_n value of PPDT2FBT increased, indicating that the macroscopic phase separation in the **PPDT2FBT$_H$**/P(NDI2OD-T2) blend was clearly suppressed.

The degree of phase separation in the PPDT2FBT:P(NDI2OD-T2) blends with different M_n was further examined by R-SoXS measurements. The R-SoXS technique can enhance the contrast between two constituent polymers and provide precise information on the degree of macroscopic phase separation.[7,15,38] Figure 5 shows the R-SoXS scattering profiles

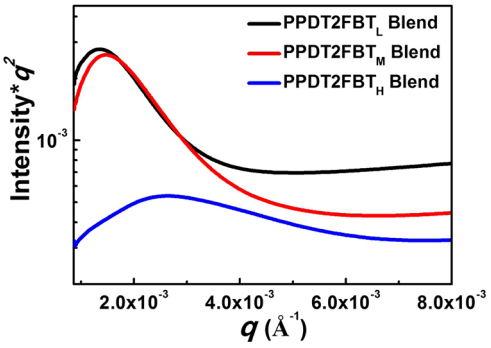

Figure 5. R-SoXS profiles of **PPDT2FBT$_L$**:P(NDI2OD-T2), **PPDT2FBT$_M$**:P(NDI2OD-T2), and **PPDT2FBT$_H$**:P(NDI2OD-T2) films prepared at the optimized device conditions.

of three different PPDT2FBT:P(NDI2OD-T2) blend films. The R-SoXS data were taken using a series of photon energies,[40] and the data acquired at 284.4 eV were used for the analysis, in which the maximum scattering contrast between the two polymers was observed. The three different PPDT2FBT:P(NDI2OD-T2) blend films showed the maximum scattering intensities at very different q values. The **PPDT2FBT$_H$**:P(NDI2OD-T2) blend had the maximum scattering intensity at q = 0.0027 Å^{-1}, whereas the **PPDT2FBT$_M$**:P(NDI2OD-T2) and **PPDT2FBT$_L$**:P(NDI2OD-T2) blended films had the maximum peak intensity at much lower q values of 0.0015 and 0.0014 Å^{-1}, respectively. This length scale represents approximately double the actual

DOI: 10.1021/ja5123182
J. Am. Chem. Soc. 2015, 137, 2359−2365

domain size, assuming that there are approximately equal volume fractions of the two respective polymer-rich domains in the blend.[10] Thus, the domain size of PPDT2FBT in **PPDT2FBT$_H$**:P(NDI2OD-T2) was calculated to be ~115 nm. In contrast, the domain sizes in **PPDT2FBT$_M$**:P(NDI2OD-T2) and **PPDT2FBT$_L$**:P(NDI2OD-T2) were approximately 210 and 225 nm, respectively, which were ~2 times larger than that in **PPDT2FBT$_H$**:P(NDI2OD-T2). Furthermore, the area under the scattering peak was the largest for the **PPDT2FBT$_L$**:P(NDI2OD-T2). This indicated that purer aggregated domains were formed in the **PPDT2FBT$_L$**:P(NDI2OD-T2), while the **PPDT2FBT$_H$**:P(NDI2OD-T2) had much better degree of intermixing.[41] These trends were supported by comparing the photoluminescence (PL) quenching efficiency of the three different blends.[42] As shown in SI Figure S4, the PL intensities of the PPDT2FBT:P(NDI2OD-T2) blends decreased significantly with increasing M_n, indicating that **PPDT2FBT$_H$**:P(NDI2OD-T2) had a larger donor/acceptor interface (i.e., smaller domain size) for facilitating photoinduced charge transfer between P(NDI2OD-T2) and PPDT2FBT at the interface.[33,43]

The results from GIXS, R-SoXS, AFM, and PL measurements suggested that tuning the M_n value of the PPDT2FBT polymers affected significantly their aggregation behavior and their blend morphology with P(NDI2OD-T2). Because both PPDT2FBT and P(NDI2OD-T2) polymers exhibit strong semicrystalline behavior, their BHJ morphology is expected to consist of three different phases, i.e., (1) PPDT2FBT domains, (2) P(NDI2OD-T2) domains, and (3) molecularly intermixed amorphous PPDT2FBT and P(NDI2OD-T2) domains, which are similar to the three phase BHJ morphologies of polymer−fullerene based systems.[44−48] In this case, the polymer acceptors or fullerenes mix in the amorphous portions of the semicrystalline polymer donors, where intimately mixed regions of donors and acceptors allow for both highly efficient exciton separation and charge-carrier extraction.[41,44,45,48−50] In addition, the aggregated pure PPDT2FBT and P(NDI2OD-T2) domains may act as hole and electron transporting pathways in the BHJ blend, respectively. Although the presence of all of these three different phases in the BHJ blend of PPDT2FBT:P(NDI2OD-T2) is an important requirement for producing efficient charge generation and transport, the strong trend of **PPDT2FBT$_L$** to form PPDT2FBT aggregates can conversely suppress the formation of the intermixed regions in PPDT2FBT:P(NDI2OD-T2) blends, resulting in reduced exciton dissociation and charge generation. In contrast, **PPDT2FBT$_H$**:P(NDI2OD-T2) may have a larger portion of **PPDT2FBT$_H$** polymers that can be intermixed molecularly with the P(NDI2OD-T2) polymers because of its lower tendency of self-aggregation.[39,44,49] In addition, the difference in the crystalline behaviors of PPDT2FBT as a function of M_n should influence the macroscopic phase separation of the PPDT2FBT:P(NDI2OD-T2) blend films. For example, the strong self-aggregating behavior of **PPDT2FBT$_L$** will induce strong polymer rod−rod interactions, i.e., the Maier−Saupe interactions,[51−54] which will drive their separation from other P(NDI2OD-T2) domains in the **PPDT2FBT$_L$**:P(NDI2OD-T2) blend. This feature has been well-documented in blends of semicrystalline polymers as well as in the assembly of semicrystalline copolymers.[51−54] In addition, the faster diffusion of the lower M_n **PPDT2FBT$_L$** could be another reason for inducing the larger phase-separated domain in the solution-processed, kinetically trapped BHJ active layer.[55]

To elucidate the relationship between the morphological changes and the performance of all-PSCs, the hole (μ_h) and electron (μ_e) mobilities of both the pristine polymer films and all-polymer blend films were measured using the space-charge-limited current (SCLC) method. SI Figure S5 and Table 2 present the measured μ_h and μ_e values. First, in the PPDT2FBT pristine films, a significant increase was observed in the μ_h values depending on the M_n value, leading to a 5-fold increase of μ_h from 4.1×10^{-5} to 1.9×10^{-4} cm^2/V s. Similar trends were also observed in the μ_h values for the PPDT2FBT:P(NDI2OD-T2) blends depending on the M_n of PPDT2FBT (Table 2). The higher μ_h value of the **PPDT2FBT$_H$** based films might be due to the stronger preference to form a "face-on" orientation, as evidenced by GIXS, which promotes efficient interchain charge transport in the vertical direction between the electrodes. Interestingly, electron transport in PPDT2FBT:P(NDI2OD-T2) was also affected by the M_n values of PPDT2FBT. In the **PPDT2FBT$_L$**:P(NDI2OD-T2) blend, the measured electron mobility (μ_e= 5.2×10^{-6} cm^2/Vs) was less than half of that of the pristine P(NDI2OD-T2) film (μ_e= 1.1×10^{-5} cm^2/V s). In contrast, the μ_e value of **PPDT2FBT$_H$**:P(NDI2OD-T2) exhibited the highest value of 1.5×10^{-5} cm^2/V s among the three different polymer blends. The combined features of the preferential face-on crystalline orientation with well-intermixed and finely separated BHJ morphology in **PPDT2FBT$_H$**:P(NDI2OD-T2) are believed to have improved the μ_h and μ_e values, thereby increasing its J_{SC} and PCE values. On the other hand, in the PPDT2FBT:P(NDI2OD-T2)-based all-PSCs, the μ_e values were still significantly lower (at least 1 order of magnitude lower) than the μ_h values, resulting in a poor μ_h/μ_e balance, which is a crucial parameter for influencing the charge recombination and the charge extraction.

Table 2. Hole and Electron Mobilities for Pristine and Blended Polymer Films by a SCLC Method[a]

sample	μ_h (cm^2/V s)	μ_e (cm^2/V s)
PPDT2FBT$_L$	4.1×10^{-5}	
PPDT2FBT$_M$	6.5×10^{-5}	
PPDT2FBT$_H$	1.9×10^{-4}	
P(NDI2OD-T2)		1.1×10^{-5}
PPDT2FBT$_L$:P(NDI2OD-T2)	7.2×10^{-5}	5.2×10^{-6}
PPDT2FBT$_M$:P(NDI2OD-T2)	1.1×10^{-4}	8.1×10^{-6}
PPDT2FBT$_H$:P(NDI2OD-T2)	2.1×10^{-4}	1.5×10^{-5}

[a]All samples were prepared at the optimized device conditions.

In this regard, an attempt was made to further optimize the photovoltaic properties of PPDT2FBT:P(NDI2OD-T2) all-PSCs by improving the μ_e value and the μ_h/μ_e balance. Diphenylether (DPE) has been used as a high-boiling point solvent additive for optimizing the thin-film morphology and improving the interchain crystalline ordering in each polymer domain.[9,30] As shown in Figure 6 and Table 3, when a small amount of DPE (1.0 vol %) was added to **PPDT2FBT$_H$**:P(NDI2OD-T2), the PCE was improved remarkably to 5.10% (V_{OC}, 0.85 V; J_{SC}, 11.90 mA cm^{-2}; and FF, 0.51), which represents one of the highest efficiencies for all-PSCs reported to date. SI Table S2 summarizes the photovoltaic parameters with different amounts of DPE. This significant enhancement of the PCE values in **PPDT2FBT$_H$**:P(NDI2OD-T2) was attributed mainly to the 33% improvement in the J_{SC} value (from 8.98 to 11.90 mA cm^{-2}). The FF value was also enhanced from 0.47 to 0.51 when the DPE additives were used.

DOI: 10.1021/ja5123182
J. Am. Chem. Soc. 2015, 137, 2359−2365

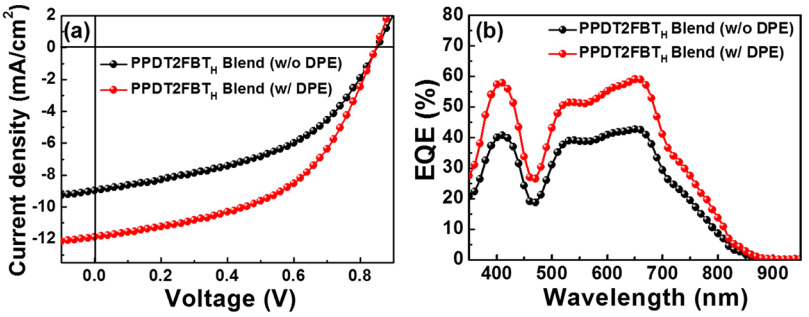

Figure 6. (a) $J-V$ characteristics and (b) EQE spectra of **PPDT2FBT$_H$**:P(NDI2OD-T2)-based all-PSCs with and without DPE.

Table 3. Photovoltaic Parameters of Three Different PPDT2FBT:P(NDI2OD-T2)-Based All-PSC Devices with DPE Additives

polymer acceptor P(NDI2OD-T2)	V_{oc} (V)	J_{sc} (mA cm^{-2})	FF	PCE$_{max}$ (%)	PCE$_{av}$[a] (%)	EQE$_{max}$ (%)	calcd J_{sc} (mA cm^{-2})
PPDT2FBT$_L$	0.86	8.88	0.51	3.88	3.78	46.9	8.47
PPDT2FBT$_M$	0.85	9.70	0.53	4.33	4.18	53.3	9.52
PPDT2FBT$_H$	0.85	11.90	0.51	5.10	5.03	59.0	12.09

[a]The average PCE value was extracted from more than 10 separated devices.

In addition, similar enhancement of the PCE value was measured for the other **PPDT2FBT$_L$**:P(NDI2OD-T2) and **PPDT2FBT$_M$**:P(NDI2OD-T2) blends after the addition of DPE (Table 3 and SI Table S3). SI Figure S6 compares the GIXS line-cut profiles for **PPDT2FBT$_H$**:P(NDI2OD-T2) without and with DPE. When DPE was added to the blend film, the degree of crystalline ordering in both the P(NDI2OD-T2) and **PPDT2FBT$_H$** polymers was improved significantly with the appearance of well-resolved diffraction peaks of (200) and (300). In addition, the face-on $\pi-\pi$ stacking distance in **PPDT2FBT$_H$**:P(NDI2OD-T2) was decreased from 3.80 to 3.72 Å by the addition of DPE, which indicates the formation of tighter interchain packing that should increase charge mobility.[19,56] Indeed, in the case of **PPDT2FBT$_H$**:P(NDI2OD-T2), DPE addition induced a remarkable increase in the μ_e values from 1.5×10^{-5} to 4.7×10^{-5} cm^2/V s, while maintaining a high hole mobility of $\sim 2 \times 10^{-4}$ cm^2/V s. Therefore, the μ_h/μ_e ratio becomes balanced from 14 to 3. Similar trends in the μ_e value and the μ_h/μ_e balance were also observed for the **PPDT2FBT$_M$** and **PPDT2FBT$_L$**-based blends (SI Figure S7 and Table S4). These results show that the incorporation of DPE could promote interchain crystalline ordering with tighter $\pi-\pi$ stacking and enhance electron transport, thereby improving the J_{SC}, FF, and PCE values of the devices.[4,9]

CONCLUSION

In conclusion, highly efficient all-PSCs showing greater than 5% PCE were demonstrated by blending **PPDT2FBT$_H$** as a donor with P(NDI2OD-T2) as an acceptor. The use of high-M_n **PPDT2FBT$_H$** was beneficial in optimizing the blend morphology for the following two reasons: (1) The preferential face-on crystalline orientation contributed to higher charge mobility in the blend film. (2) The higher tendency of intermixing between **PPDT2FBT$_H$** and P(NDI2OD-T2) with a smaller domain size contributed to the improvement in both the charge separation efficiency and the charge transport in the blend film. Therefore, the M_n of the polymers is interpreted as a principal factor that finely controls the BHJ morphology, i.e., self-organization and intermixing of polymer donor and acceptor, which influenced the photovoltaic characteristics significantly in the PPDT2FBT:P(NDI2OD-T2) based all-PSC devices. In addition, the incorporation of DPE additive provides an efficient means of further enhancing the charge carrier mobility by improving the crystalline ordering with tighter $\pi-\pi$ stacking in each polymer domain. Therefore, the use of a high-M_n **PPDT2FBT$_H$** donor produced high J_{SC} ($\sim$12 mA cm^{-2}) and FF values (>0.5) in all-PSCs (PCE = 5.10%). The findings from this model system provide the guidelines for choosing the optimal polymer donor and acceptor pairs as well as their molecular weight for highly efficient all-PSCs.

ASSOCIATED CONTENT

Supporting Information

Materials and methods, detailed experimental procedures, and additional characterization data. This material is available free of charge via the Internet at http://pubs.acs.org.

AUTHOR INFORMATION

Corresponding Authors

bumjoonkim@kaist.ac.kr
hywoo@pusan.ac.kr

Author Contributions

[‖]These authors contributed equally.

Notes

The authors declare no competing financial interest.

ACKNOWLEDGMENTS

This research was supported by the National Research Foundation Grant (2012M3A6A7055540, 2013R1A2A1A03069803, 2012R1A1A2005855), funded by the Korean Government. This research was supported by the New & Renewable Energy Program of KETEP Grant (20133030011330), funded by the Ministry of Trade, Industry & Energy, Republic of Korea. We thank Prof. Gila Stein for helpful discussions. The Advanced Light Source is supported by the U.S. Department of Energy under Contract No. DE-AC02-05CH11231.

REFERENCES

(1) Facchetti, A. *Mater. Today* **2013**, *16*, 123–132.

DOI: 10.1021/ja5123182
J. Am. Chem. Soc. 2015, 137, 2359–2365

(2) Earmme, T.; Hwang, Y.-J.; Murari, N. M.; Subramaniyan, S.; Jenekhe, S. A. *J. Am. Chem. Soc.* **2013**, *135*, 14960−14963.
(3) Mori, D.; Benten, H.; Okada, I.; Ohkita, H.; Ito, S. *Energy Environ. Sci.* **2014**, *7*, 2939−2943.
(4) Zhou, E.; Cong, J.; Hashimoto, K.; Tajima, K. *Adv. Mater.* **2013**, *25*, 6991−6996.
(5) Li, W.; Roelofs, W. S. C.; Turbiez, M.; Wienk, M. M.; Janssen, R. A. J. *Adv. Mater.* **2014**, *26*, 3304−3309.
(6) Zhou, N.; Lin, H.; Lou, S. J.; Yu, X.; Guo, P.; Manley, E. F.; Loser, S.; Hartnett, P.; Huang, H.; Wasielewski, M. R.; Chen, L. X.; Chang, R. P. H.; Facchetti, A.; Marks, T. J. *Adv. Energy Mater.* **2014**, DOI: 10.1002/aenm.201300785.
(7) Zhou, Y.; Kurosawa, T.; Ma, W.; Guo, Y.; Fang, L.; Vandewal, K.; Diao, Y.; Wang, C.; Yan, Q.; Reinspach, J.; Mei, J.; Appleton, A. L.; Koleilat, G. I.; Gao, Y.; Mannsfeld, S. C. B.; Salleo, A.; Ade, H.; Zhao, D.; Bao, Z. *Adv. Mater.* **2014**, *26*, 3767−3772.
(8) Jung, I. H.; Lo, W.-Y.; Jang, J.; Chen, W.; Zhao, D.; Landry, E. S.; Lu, L.; Talapin, D. V.; Yu, L. *Chem. Mater.* **2014**, *26*, 3450−3459.
(9) Kang, H.; Kim, K.-H.; Choi, J.; Lee, C.; Kim, B. J. *ACS Macro Lett.* **2014**, *3*, 1009−1014.
(10) Mu, C.; Liu, P.; Ma, W.; Jiang, K.; Zhao, J.; Zhang, K.; Chen, Z.; Wei, Z.; Yi, Y.; Wang, J.; Yang, S.; Huang, F.; Facchetti, A.; Ade, H.; Yan, H. *Adv. Mater.* **2014**, *26*, 7224−7230.
(11) Earmme, T.; Hwang, Y.-J.; Subramaniyan, S.; Jenekhe, S. A. *Adv. Mater.* **2014**, *26*, 6080−6085.
(12) Holcombe, T. W.; Woo, C. H.; Kavulak, D. F. J.; Thompson, B. C.; Fréchet, J. M. J. *J. Am. Chem. Soc.* **2009**, *131*, 14160−14161.
(13) Lin, Y.; Zhan, X. *Mater. Horiz.* **2014**, *1*, 470−488.
(14) Zhou, E.; Cong, J.; Wei, Q.; Tajima, K.; Yang, C.; Hashimoto, K. *Angew. Chem., Int. Ed.* **2011**, *50*, 2799−2803.
(15) Schubert, M.; Collins, B. A.; Mangold, H.; Howard, I. A.; Schindler, W.; Vandewal, K.; Roland, S.; Behrends, J.; Kraffert, F.; Steyrleuthner, R.; Chen, Z.; Fostiropoulos, K.; Bittl, R.; Salleo, A.; Facchetti, A.; Laquai, F.; Ade, H. W.; Neher, D. *Adv. Funct. Mater.* **2014**, *24*, 4068−4081.
(16) Schubert, M.; Dolfen, D.; Frisch, J.; Roland, S.; Steyrleuthner, R.; Stiller, B.; Chen, Z.; Scherf, U.; Koch, N.; Facchetti, A.; Neher, D. *Adv. Energy Mater.* **2012**, *2*, 369−380.
(17) Liu, X.; Huettner, S.; Rong, Z.; Sommer, M.; Friend, R. H. *Adv. Mater.* **2012**, *24*, 669−674.
(18) Veenstra, S. C.; Loos, J.; Kroon, J. M. *Prog. Photovolt.: Res. Appl.* **2007**, *15*, 727−740.
(19) Hwang, Y.-J.; Earmme, T.; Subramaniyan, S.; Jenekhe, S. A. *Chem. Commun.* **2014**, *50*, 10801−10804.
(20) Kline, R. J.; McGehee, M. D.; Kadnikova, E. N.; Liu, J.; Fréchet, J. M. J.; Toney, M. F. *Macromolecules* **2005**, *38*, 3312−3319.
(21) Goh, C.; Kline, R. J.; McGehee, M. D.; Kadnikova, E. N.; Frechet, J. M. J. *Appl. Phys. Lett.* **2005**, *86*, 122110.
(22) Schilinsky, P.; Asawapirom, U.; Scherf, U.; Biele, M.; Brabec, C. J. *Chem. Mater.* **2005**, *17*, 2175−2180.
(23) Cho, S.; Seo, J. H.; Park, S. H.; Beaupré, S.; Leclerc, M.; Heeger, A. J. *Adv. Mater.* **2010**, *22*, 1253−1257.
(24) Müller, C.; Wang, E.; Andersson, L. M.; Tvingstedt, K.; Zhou, Y.; Andersson, M. R.; Inganäs, O. *Adv. Funct. Mater.* **2010**, *20*, 2124−2131.
(25) Chu, T.-Y.; Lu, J.; Beaupré, S.; Zhang, Y.; Pouliot, J.-R.; Zhou, J.; Najari, A.; Leclerc, M.; Tao, Y. *Adv. Funct. Mater.* **2012**, *22*, 2345−2351.
(26) Lee, H. K. H.; Li, Z.; Constantinou, I.; So, F.; Tsang, S. W.; So, S. K. *Adv. Energy Mater.* **2014**, DOI: 10.1002/aenm.201400768.
(27) Intemann, J. J.; Yao, K.; Yip, H.-L.; Xu, Y.-X.; Li, Y.-X.; Liang, P.-W.; Ding, F.-Z.; Li, X.; Jen, A. K. Y. *Chem. Mater.* **2013**, *25*, 3188−3195.
(28) Liu, C.; Wang, K.; Hu, X.; Yang, Y.; Hsu, C.-H.; Zhang, W.; Xiao, S.; Gong, X.; Cao, Y. *ACS Appl. Mater. Interfaces* **2013**, *5*, 12163−12167.
(29) Mori, D.; Benten, H.; Ohkita, H.; Ito, S.; Miyake, K. *ACS Appl. Mater. Interfaces* **2012**, *4*, 3325−3329.
(30) Nguyen, T. L.; Choi, H.; Ko, S. J.; Uddin, M. A.; Walker, B.; Yum, S.; Jeong, J. E.; Yun, M. H.; Shin, T. J.; Hwang, S.; Kim, J. Y.; Woo, H. Y. *Energy Environ. Sci.* **2014**, *7*, 3040−3051.
(31) Yan, H.; Chen, Z.; Zheng, Y.; Newman, C.; Quinn, J. R.; Dotz, F.; Kastler, M.; Facchetti, A. *Nature* **2009**, *457*, 679−686.
(32) Steyrleuthner, R.; Schubert, M.; Jaiser, F.; Blakesley, J. C.; Chen, Z.; Facchetti, A.; Neher, D. *Adv. Mater.* **2010**, *22*, 2799−2803.
(33) Mori, D.; Benten, H.; Okada, I.; Ohkita, H.; Ito, S. *Adv. Energy Mater.* **2014**, DOI: 10.1002/aenm.201301006.
(34) Chen, M. S.; Niskala, J. R.; Unruh, D. A.; Chu, C. K.; Lee, O. P.; Fréchet, J. M. J. *Chem. Mater.* **2013**, *25*, 4088−4096.
(35) Rivnay, J.; Mannsfeld, S. C. B.; Miller, C. E.; Salleo, A.; Toney, M. F. *Chem. Rev.* **2012**, *112*, 5488−5519.
(36) Kim, K.-H.; Park, S.; Yu, H.; Kang, H.; Song, I. H.; Oh, J. H.; Kim, B. J. *Chem. Mater.* **2014**, *26*, 6963−6970.
(37) Osaka, I.; Saito, M.; Koganezawa, T.; Takimiya, K. *Adv. Mater.* **2014**, *26*, 331−338.
(38) Yan, H.; Collins, B. A.; Gann, E.; Wang, C.; Ade, H.; McNeill, C. R. *ACS Nano* **2011**, *6*, 677−688.
(39) Pavlopoulou, E.; Kim, C. S.; Lee, S. S.; Chen, Z.; Facchetti, A.; Toney, M. F.; Loo, Y.-L. *Chem. Mater.* **2014**, *26*, 5020−5027.
(40) Gann, E.; Young, A. T.; Collins, B. A.; Yan, H.; Nasiatka, J.; Padmore, H. A.; Ade, H.; Hexemer, A.; Wang, C. *Rev. Sci. Instrum.* **2012**, *83*, 045110.
(41) Collins, B. A.; Li, Z.; Tumbleston, J. R.; Gann, E.; McNeill, C. R.; Ade, H. *Adv. Energy Mater.* **2013**, *3*, 65−74.
(42) Kim, K.-H.; Kang, H.; Kim, H. J.; Kim, P. S.; Yoon, S. C.; Kim, B. J. *Chem. Mater.* **2012**, *24*, 2373−2381.
(43) Bloking, J. T.; Giovenzana, T.; Higgs, A. T.; Ponec, A. J.; Hoke, E. T.; Vandewal, K.; Ko, S.; Bao, Z.; Sellinger, A.; McGehee, M. D. *Adv. Energy Mater.* **2014**, DOI: 10.1002/aenm.201301426.
(44) Bartelt, J. A.; Beiley, Z. M.; Hoke, E. T.; Mateker, W. R.; Douglas, J. D.; Collins, B. A.; Tumbleston, J. R.; Graham, K. R.; Amassian, A.; Ade, H.; Fréchet, J. M. J.; Toney, M. F.; McGehee, M. D. *Adv. Energy Mater.* **2013**, *3*, 364−374.
(45) Jamieson, F. C.; Domingo, E. B.; McCarthy-Ward, T.; Heeney, M.; Stingelin, N.; Durrant, J. R. *Chem. Sci.* **2012**, *3*, 485−492.
(46) Yin, W.; Dadmun, M. *ACS Nano* **2011**, *5*, 4756−4768.
(47) Graham, K. R.; Cabanetos, C.; Jahnke, J. P.; Idso, M. N.; El Labban, A.; Ngongang Ndjawa, G. O.; Heumueller, T.; Vandewal, K.; Salleo, A.; Chmelka, B. F.; Amassian, A.; Beaujuge, P. M.; McGehee, M. D. *J. Am. Chem. Soc.* **2014**, *136*, 9608−9618.
(48) Sweetnam, S.; Graham, K. R.; Ngongang Ndjawa, G. O.; Heumüller, T.; Bartelt, J. A.; Burke, T. M.; Li, W.; You, W.; Amassian, A.; McGehee, M. D. *J. Am. Chem. Soc.* **2014**, *136*, 14078−14088.
(49) Westacott, P.; Tumbleston, J. R.; Shoaee, S.; Fearn, S.; Bannock, J. H.; Gilchrist, J. B.; Heutz, S.; deMello, J.; Heeney, M.; Ade, H.; Durrant, J.; McPhail, D. S.; Stingelin, N. *Energy Environ. Sci.* **2013**, *6*, 2756−2764.
(50) Vakhshouri, K.; Kozub, D. R.; Wang, C.; Salleo, A.; Gomez, E. D. *Phys. Rev. Lett.* **2012**, *108*, 026601.
(51) Pryamitsyn, V.; Ganesan, V. *J. Chem. Phys.* **2004**, *120*, 5824−5838.
(52) Rathi, P.; Huang, T.-M.; Dayal, P.; Kyu, T. *J. Phys. Chem. B* **2008**, *112*, 6460−6466.
(53) Olsen, B. D.; Shah, M.; Ganesan, V.; Segalman, R. A. *Macromolecules* **2008**, *41*, 6809−6817.
(54) Kim, H. J.; Paek, K.; Yang, H.; Cho, C.-H.; Kim, J.-S.; Lee, W.; Kim, B. J. *Macromolecules* **2013**, *46*, 8472−8478.
(55) Gilmore, P. T.; Falabella, R.; Laurence, R. L. *Macromolecules* **1980**, *13*, 880−883.
(56) Steyrleuthner, R.; Di Pietro, R.; Collins, B. A.; Polzer, F.; Himmelberger, S.; Schubert, M.; Chen, Z.; Zhang, S.; Salleo, A.; Ade, H.; Facchetti, A.; Neher, D. *J. Am. Chem. Soc.* **2014**, *136*, 4245−4256.

DOI: 10.1021/ja5123182
J. Am. Chem. Soc. 2015, 137, 2359−2365